International Journal of Metallurgical Engineering 2013, 2(1): 100-110
DOI: 10.5923/j.ijmee.20130201.15

Role of Base Metal Microstructure on Tensile Properties and Weldability of Simulated Continuously Annealed Advanced High Strength Steels

Kumkum Banerjee

R&D Dept, Tata Steel Limited, Jamshedpur, India

Abstract Advanced high strength steels (AHSS) are several families of steels (dual phase, transformation-induced plasticity, complex phase and martensitic steels) that constitute ferrite along with low temperature phases--martensite, bainite and/or retained austenite, in adequate quantities, to obtain desired mechanical properties. These steels find their applications in automobiles and are able to enhance mechanical properties with reduced weight that make them cost effective, fuel efficient and environment friendly. All AHSS are produced using proper chemistry design in association with controlled rate of cooling from the austenite–ferrite phase region, either on the run-out table in a hot rolling mill or in the cooling section of a continuous annealing line. This ensures high strength and other desired properties essentially through the low temperature phase transformation products. In the present investigation, the base metal microstructure had played a key role in dictating tensile properties and weldability of spot welded AHSS in simulated continuously annealed conditions. A few miocroalloyed AHSS with low carbon equivalent were produced in a laboratory air induction furnace and were subsequently hot forged and rolled in the laboratory. Continuous heating and cooling transformations were vividly studied in a Gleeble 1500D to determine intercritical temperature regimes and the transformation temperatures in association with cooling rates of the low temperature transformation products. The hot rolled samples after duly cold rolled were submitted to strip annealing simulation to mimic actual continuous annealing, employing a Gleeble 3500 thermomechanical simulator. Two types of annealing cycles were simulated to examine the effect of cooling rate and bainite alongside fine microalloying precipitates on tensile properties and weldability. The annealing cycles that resulted in ferrite, 37% bainite and martensite in association with nano-sized Mo-C were successful in delivering the satisfactory combination of tensile properties and weldability.

Keywords Advanced High Strength Steel, Continuous Annealing, Microalloying Precipitates, Haz Softening, Tensile Strength, Ductility, Resistance Spot Welding, Weldability

1. Introduction

In recent years, light-weight-fuel-efficient vehicles that ensure passenger safety have become a priority for automotive industries. Manufacturing of such vehicles has been possible by the development of high strength multiphase advanced high strength (AHSS) steels. AHSS is a term used to describe several families of steels (dual phase-DP, transformation induced plasticity—TRIP, complex phase–CP and martensitic steels) that contain ferrite, martensite, bainite and/or retained austenite in sufficient quantities to produce desired mechanical properties. Some types of AHSS have higher strain hardening capacity resulting in strength-ductility balance that is superior to conventional steels while other types possess ultrahigh yield and tensile strength in association with bake hardening behaviour[1]. All AHSS are produced by controlling the cooling rate from the austenite –ferrite phase, either on the run-out table of the hot rolling mill or in the cooling section of the continuous annealing line to ensure high strength levels through bainitic-martensitic transformation[2]. However, such transformations can not be achieved unless the cooling rate is over a critical threshold that depends on steel composition[3]. The critical cooling rate increases with decreasing alloying additions and as the cooling rates attainable by industries are limited, without the addition of alloying elements, achievement of high strength is not possible.

Problems in welding AHSS

Generally, sheet steels can be hardened by the addition of C, Si, Mn, P etc. However, increasing alloying elements, such as C, Si and Mn enhances quenching hardenability of steels that affects weldability adversely[2-5]. Weldability of steels depends upon carbon equivalent (CE) that gives the measure of hardenability of the steel and is a function of

* Corresponding author:
kumkum.banerjee@tatasteel.com (Kumkum Banerjee)
Published online at http://journal.sapub.org/ijmee
Copyright © 2013 Scientific & Academic Publishing. All Rights Reserved

alloying elements present.

The following expression is widely used for expressing CE of AHSS[6].

CE = C + Si/30 +Mn/20+2P+4S (mass%)

Resistance spot welding is a favoured method for joining advanced high strength steels[7]. The welding lobes of AHSS are narrower than mild and high strength steels. Further, AHSS tend to exhibit higher expulsion, higher electrode wear and most importantly, they fail during pull button test resulting in interfacial failure. The acceptable strength is achievable in these spot welded steels with full button pull, partial button pull or partial interfacial fracture.

Several researchers on AHSS have reported the welding related problems for the formation of matensite in the weld nugget[8, 9]. Martensite can also form in resistance spot welds, even at low carbon levels as cooling rate associated with spot welding[10, 11] is quite high. Similar observations were made while laser beam welding (LBW) was conducted on AHSS

[12, 13]. The hardness achieved in the steels is directly associated with the fast cooling in the welding processes that can achieve cooling rate of the order of 10^3-10^5 ^{o}C/s[5,14]. The hard martensite thus formed due to high cooling rate, provides a path for a crack to propagate. In addition, rapid cooling can cause porosities towards the edges of the weld where stress concentration is highest in a peel test[15] and also solidification cracking enhancing the chances of interfacial failure of a spot weld[14].

Shrinkage, solidification cracks and liquid metal embrittlement in DP 600 were also observed by Milititsky et al[16] in some welds, where weld current and hold time were found responsible for the formation of such imperfections. In another work[17], the detection and prediction of expulsion during spot welding of DP600 were reported. Several researchers have reported about the interfacial failures in DP600 steel while the weld size exceeded the minimum threshold size[189]. In addition, Wang et al. also found interfacial fracture in DP600 steel weld buttons for the thicker gages[19-21]. Such failures were attributed to solidification cracks and shrinkage voids[22].

It can be mentioned that HAZ softening may occur in the case of AHSS with significant amount of martensite[23, 24] in the base metal that can be attributed to martensite tempering at the points of the weld where the temperature approached A1 (subcritical HAZ). Further, as DP steel essentially derive its strength from the composite microstructure of ferrite and martensite and as martensite is a thermally unstable phase, it tends to decompose in the heat affected zone (HAZ) resulting in softening and thus causing hardness reduction. This phenomenon is termed as HAZ softening[25, 26]. HAZ softening is a very complex phenomenon that is affected by steel composition, base metal martensite content, prestrain and heat input[27-29] and it can have detrimental impact on weldment. HAZ softening was also reported by Dancette et al[30, 18] in DP980 due to martensite tempering, however, the presence of a low amount of martensite in the base metal of DP450, helped avoid HAZ softening.

In this article, a detailed discussion on the role of base metal microstructure on tensile properties and weldability of the steels is presented.

2. Experimental

2.1. Material

Two heats were made using a 25-kg in-house laboratory air induction furnace. Chemical composition (in wt%) of the heats (Heat Nos. 9 and 14) along with the carbon equivalents are presented in Table 1.

Table 1. Chemical composition and carbon equivalent of the developed steels

Heat No.	C	Mn	Si	Al	Mo	Ti	Nb	Cr	P	S	CE
9	0.12	1.52	0.37	0.15	0.29	0.009	0.004	0.021	0.008	0.013	0.27
14	0.09	1.55	0.41	0.27	0.21	0.031	0.009	0.036	0.008	0.008	0.24

2.2. Hot Rolling

Equilibrium transformation temperatures (Ae1 and Ae3) for the steels were calculated using Thermo-Calc (TCFE3) so that finish rolling temperatures remained 30-40^{o}C above the A3 temperatures. The ingots were forged at 1200^{o}C for 2 hrs. and subsequently hot rolled by soaking at 1200^{o}C for 1-hr in a furnace at RDCIS SAIL, Ranchi. The Ae3 temperature of the steels is 847-850^{o}C, while the finish rolling temperatures (FRT) of the steels 9, 10 and 14 were 875, 862 and 885^{o}C, respectively.

2.3. Dilatometry

For designing continuous annealing cycles, AC_1 and AC_3 temperatures were determined by continuous heating and Bs/Ms temperatures through continuous cooling transformation (CHT & CCT) tests on Gleeble 1500D thermomechanical simulator using 80mm long-3mm-dia samples from hot rolled materials.

For CHT, samples were heated at the rate of 1-100^{o}C/s to 1050^{o}C, followed by air cooling. While, for CCT, samples were heated to 1050^{o}C for 2-mins. at the rate of 5^{o}C/s, followed by cooling at the rate of 0.5^{o}C/s-100^{o}C/s.

For microstructural analysis of the CCT samples, all samples were cut in half, approximately at the position of the thermocouple and were prepared for metallographic examination following standard sample preparation technique, while using 2% nital to reveal microstructures.

2.4. Continuous Annealing Simulation

The hot rolled samples were cold rolled to ~ 0.8-1 mm using the laboratory cold rolling set-up at NML Jamshedpur for subsequent continuous annealing (CAL) simulation. To simulate continuous annealing cycles, strip annealing facility of RDCIS, SAIL Ranchi was utilized. The strip samples of 260mmX50mm were used for the annealing simulation.

The simulation was carried out in the intercritical temperature range ($\alpha+\gamma$) that was determined by CHT tests on Gleeble 1500D. Two types of continuous annealing cycles were designed for strip annealing simulation on Gleeble 3500 to examine the effect of cooling rate and bainite on tensile properties and weldability.

2.5. Effect of Cooling Rate

Cold rolled samples of Heat-14 were used to examine the effects of cooling rate in the simulated annealing cycles. The parameters used in the annealing cycles along with their thermal cycles are given in Table 2.

Table 2. Annealing parameters for cooling rate effect

Anneal. cycle	Heating rate, °C/sec	Soaking temp., °C	Soaking time, sec	Slow cooling rate, °C/sec	Fast cooling temp., °C	Fast cooling rate, °C/s
14-CR-1	10	830	120	2	800	100
14-CR-2	10	830	120	2	800	30

2.6. Effect of Bainite

Cold rolled samples of Heat-9 were used to examine the effects bainite in the simulated annealing cycles. The parameters used in the annealing cycles along with their thermal cycles are given in Table 3.

Table 3. Annealing parameters for bainite effect

Anneal. cycle	Heating rate,°C/s	Soaking temp., °C	Soaking time, sec	Slow cooling rate, °C/s	Fast cooling temp, °C	Fast cooling rate, °C/s	Bainite temp., °C	Bainite time, sec	Cooling rate,°C/s
9-B-1	10	780	60	2	760	40	470	60	70
9-B-2	10	780	120	2	760	20	470	60	10

2.7. Welding of Annealed Samples

A DC MF-90 Spot Welder was used to spot weld the annealed samples using a Cu-Cr-Zr alloyed electrode of 5-mm truncated tip diameter. The squeeze force, weld current and weld time were 22daN, 5.8-6kN and 180-200s, respectively. After welding, the samples were submitted for peel-testing using a laboratory vice.

2.8. Microscopy, Hardness Measurements and Tensile Testing (Hot Bands, Annealed Samples and Welded Samples)

Cross sections of samples after hot rolling, cold-rolled-annealing and welding were ground and polished following standard metallographic procedures. Thereafter, the samples were examined by optical (OM), high resolution scanning electron microscopy (FEG-SEM) and transmission electron microscopy (TEM) equipped with energy dispersive spectroscopes (EDS). For OM and FEG-SEM, the polished specimens were etched with 2% nital. For TEM, thin foils of 3-mm diameter were punched from mechanically thinned ~60 mm slices and were electro-polished in a solution of methanol and 10% perchloric acid at -40°C using a twin-jet electropolisher. Thin foils were examined using a Phillips CM12 transmission electron microscope operated at 120kV.

Microhardness measurements of various phases present in the hot bands and the CCT samples were conducted using LECO LM 247AT Vickers microhradness tester, while macro hardness for the hot bands and resistance spot weldments were measured using a LECO LV700AT Vickers Hardness tester.

The annealed samples were further submitted to tensile testing following ASTME-08 sample dimension on Instron 5582 tensile tester to record the tensile data.

3. Results and Discussion

3.1. Hot Band Microstructure

The microstructure of hot band-9 (Heat-9) consisted of ferrite and pearlite (Fig 1a) in association with nano-sized Mo-C carbides (Fig. 1b, c). On the other hand, hot band-14 consisted of ferrite, pearlite, bainite and martensite (Fig.2a). Further, complex precipitates (Ti-Nb-Mo) C (Fig. 2b, c), rich in Ti were also observed in hot band-14 as Ti content was higher (0.031) in this band than that of the hot band-9 (0.009). The ferrite grain size of the hot bands 9 and 14 were 4.1 and 3.7 μm, while ferrite area fractions were 69 and 79, respectively.

3.2. Continuous Cooling Transformation

Heat-9

From continuous cooling transformation it was observed

that below 5°C/s cooling rate, ferrite, pearlite and bainite were present, while between 5°C/s and 20°C/s, the co-existence of ferrite and bainite were noticed. Further increase in cooling rate till 70°C/s showed the presence of martensite in association with ferrite and bainite, while above 70°C/s, bainite disappeared and only ferrite and martensite were present.

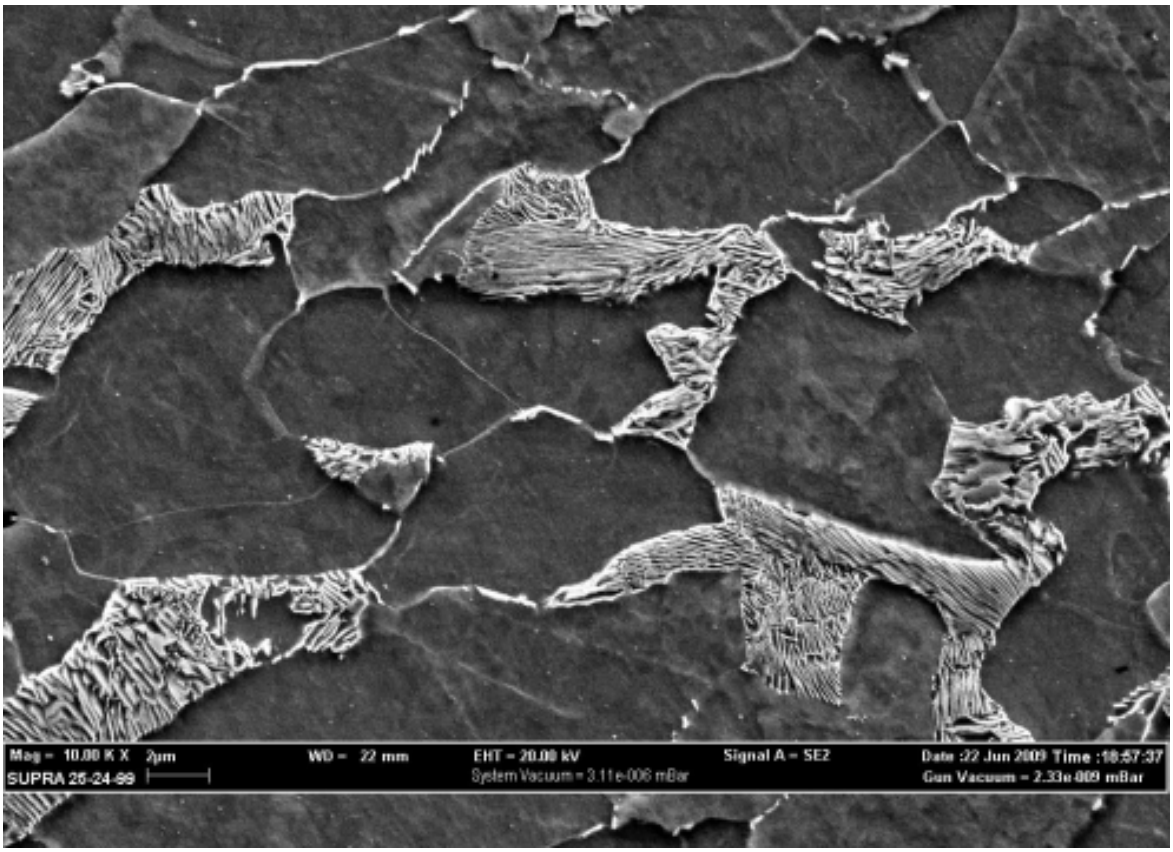

(a)

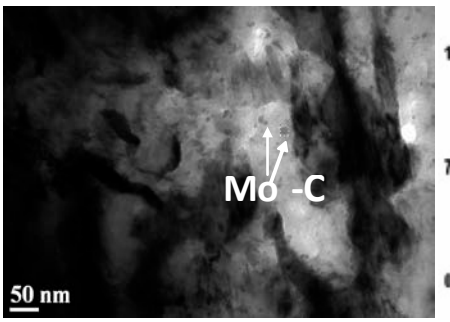

(b)

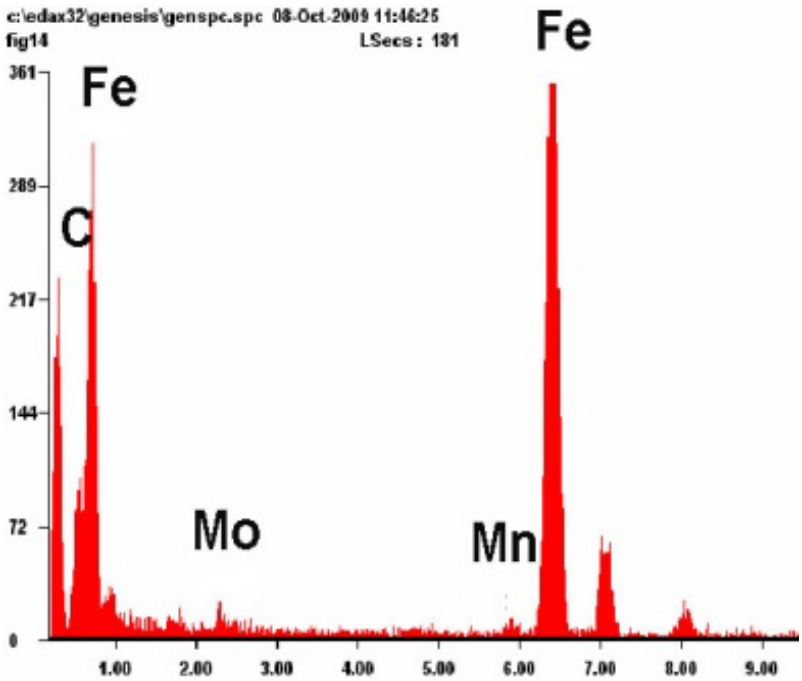

(c)

Figure 1. **(a)** FEG-SEM micrographs showing ferritic-pearlitic structure, **(b)**TEM micrograph showing nano-sized Mo-C precipitates and **(c)** EDS of the precipitates in the hot band of Heat-9

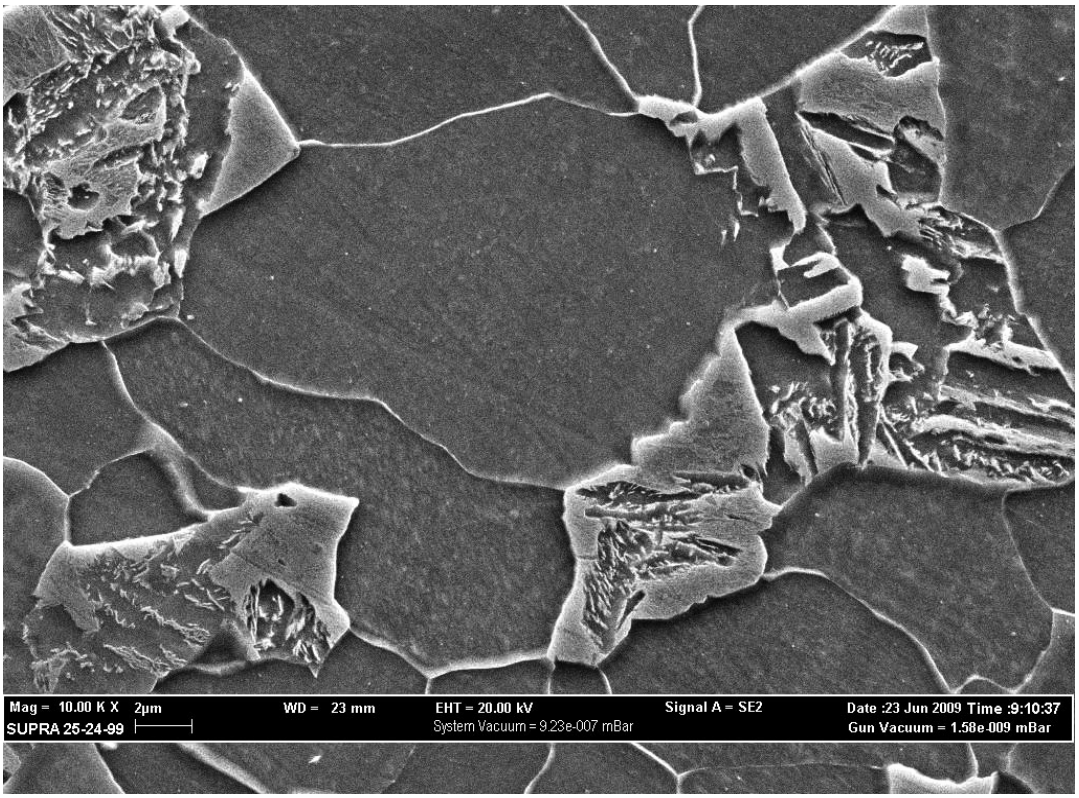

(a)

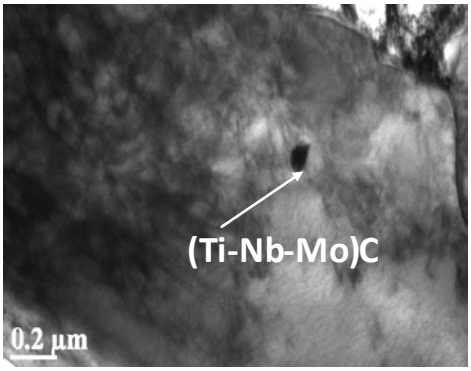

(b)

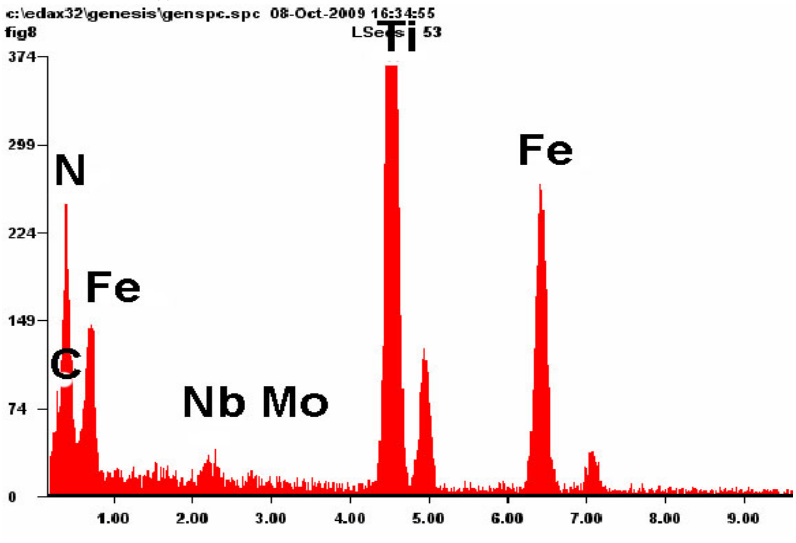

(c)

Figure 2. (a) FEG-SEM micrographs showing ferritic-banitic-martensitic structure **(b)** TEM micrograph showing (Ti-Nb-Mo)C precipitates **(c)** EDS of the precipitates in the hot band of Heat-14

Heat- 14

In Heat-14, pearlite was observed in association with ferrite and bainite in the cooling rate range of 10-20^{o}C/s, while till 10^{o}C/s ferrite structure was dominant. While from 20 to 100^{o}C/s, ferrite, bainite and martensite were present.

For designing continuous annealing cycles, fast cooling rate was maintained to avoid pearlite formation as the presence of pearlite develops yield point elongation and which in turn causes surface problems. Thus, from the CCT studies, the cooling rate for Heat-9 was kept above 5^{o}C/s, while for Heat-14, the cooling rate maintained was above 20^{o}C/s.

3.3. Continuously Annealed Samples

Effect of cooling rate—Annealing cycles 14-CR-1 and 14-CR-2

a) Microstructure

Samples that underwent cycles 14-CR-1: 10^{o}C/s—830^{o}C (120s)-2^{o}C/s-800^{o}C-100^{o}C/s and 14-CR-2: 10^{o}C/s—850^{o}C

(120s)-2°C/s-800°C-30°C/s, experienced cooling rates of 100 and 30°C/s, respectively. In both the samples ferritic-martensitic microstructure was obtained with 40% and 31% martensite fraction, respectively (Figs. 3a, b). Due to the fast cooling rate of 100 °C/s, no new precipitates could be formed during the cooling cycle of 14-CR-1, however, as the cooling rate in 14-CR-2 was slower (30°C/s), some TiC precipitates were also formed (Fig. 3c). Further, the presence of (Ti-Nb-Mo) CN precipitates was also observed in 14-CR-2.

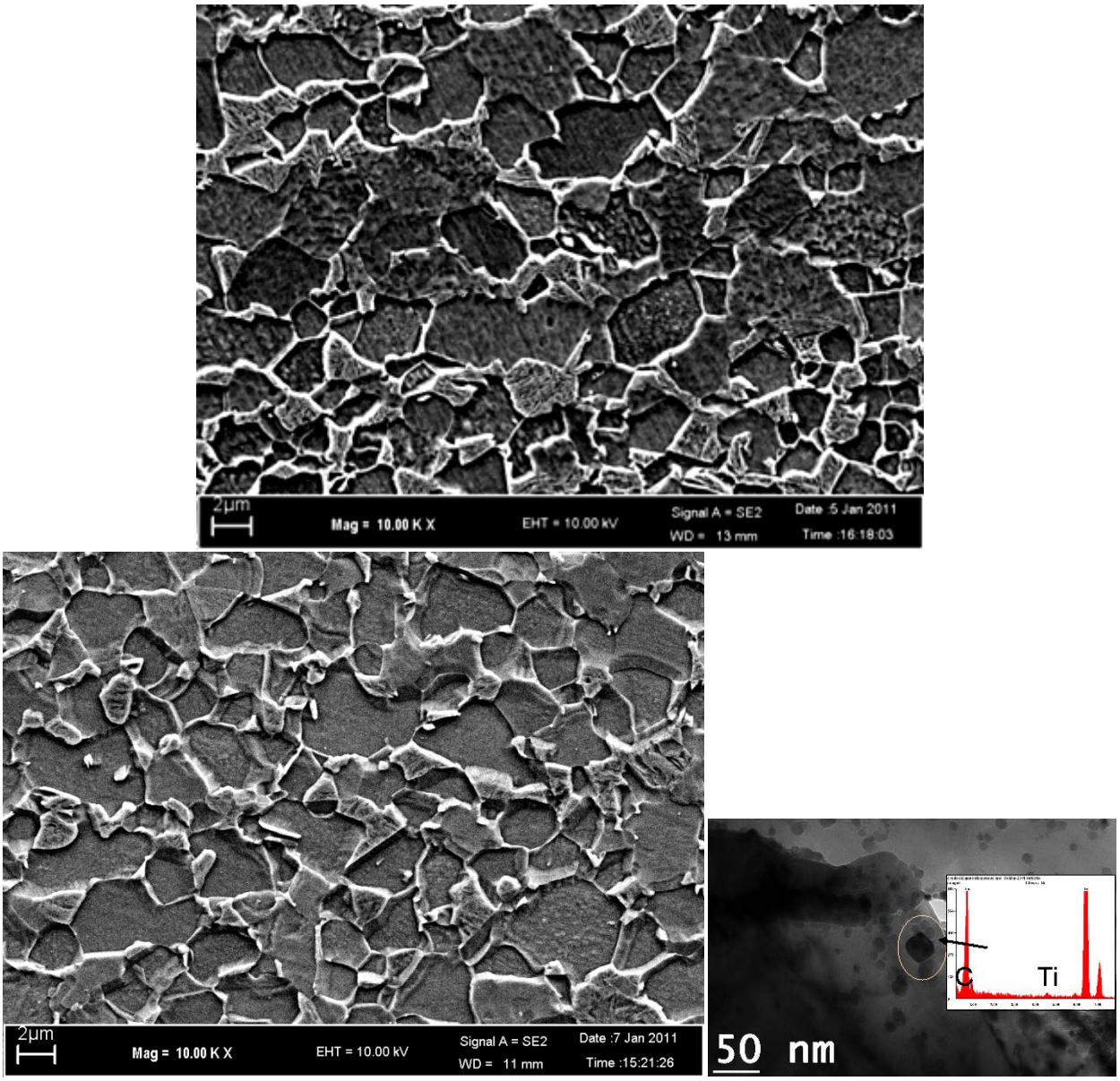

Figure 3. (a,b) FEG-SEM micrographs showing ferritic-martensitic structures for annealing cycles 14-CR-1 and 2, respectively and (c) showing the EDS of TiC precipitate in 14-CR-2 sample

b) Tensile properties

The YS and UTS of cold-rolled and continuously annealed 14-CR-1 were registered as 405 MPa (Table 4) and 750 MPa, respectively, with % UEL (%Uniform Elongation) of 13% and %TEL (%Total Elongation) of 19% for 100°C/s cooling rate The precipitates helped increase the YS to 494 MPa compared to 405 MPa in 14-CR-1, by grain refinement and restricting dislocation movement. However, UTS was reduced to 690 MPa for 14-CR-2, as martensite content reduced, while %UEL and TEL were increased to 17% and 27%, respectively. The strain hardening exponents (n) for 14-CR-1 and 2 were satisfactory with 0.18 and 0.20, respectively.

Table 4. Microstructure, tensile data and weld quality of simulated continuously annealed samples

Sample	Microstructure	YS, MPa	UTS, MPa	% UEL	% TEL	n	Weld quality
Cycle-14-CR-1	F+40% M	405	750	13	19	0.18	Porosities in weld zone and cracks in HAZ
Cycle-14-CR-2	F+31%M and TiC precipitate	494	690	17	27	0.20	No porosities and cracks in weldment
Cycle-9-B-1	F+ 25%(M+ B)	600	702	16	23	0.23	HAZ cracks
Cycle-9-B-2	F+37%(B+M) and Mo-C precipitate	449	753	16	22	0.18	No porosities and cracks in weldment

c) Weldability

The welded sample of 14-CR-1 showed plug type nugget failure with predominantly martensitic in association with bainitic welded structure (Fig.4a,b--representative photographs are presented as in all the cases failure was plug type with predominantly martensitic weld structure). The weld zone was examined by FEG-SEM and porosities were observed. Further, the cracks initiated in a zone where the alloy remained in the solidus-liquidus temperature range during welding. The dendrite structure inside open cracks (Fig. 4c) indicates that the liquid was present at the moment of crack formation and therefore, it is liquation cracking according to the classification of Hemsworth et al[31]. In addition, cracking in the heat affected zone also was initiated by the presence of MnS stringers (Fig. 4c). This can be attributed to the triaxial stresses at the sharp corners of the stringers during cooling cycle of the welding. This helped lower the cohesive force at the MnS-matrix interface and thus initiated a crack. While hardness values for the weld, HAZ and base metal were 309, 256 and 290 VPN, respectively. Thus, hardness of the HAZ was quite lower than that of the weld region and base metal that is indicative of the fact that the HAZ softening was the possible reason for the HAZ cracking and poor weldability. The HAZ softening occurred in this case while significant amount of martensite (40%) was present in the base metal, which was in good agreement with the conclusion made in the literature[23, 24]. In HAZ softening, martensite tempering takes place at the points of the weld where the temperate approaches A1 (subcritical HAZ). This is because a hard weld metal can not deform plastically to release welding stresses and they are transferred to the softened HAZ, causing it to crack[32]. This is the reason why softer base metal consistently suffers a smaller amount of HAZ cracking than the harder consisting of large amount of martensite.

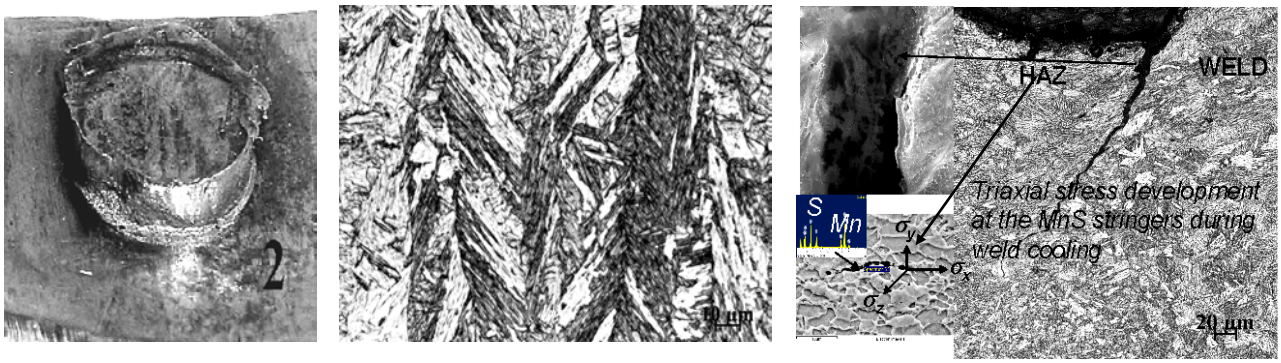

Figure 4. **(a)** Showing a representative photograph of pullout button failure, **(b)** showing OM micrograph of predominantly martensitic structure in weld zone **(c)** OM micrograph showing liquation crack in the fusion line[FEG-SEM magnified view in the top-left inset] along with HAZ crack at the Mn-S stringers[bottom-left inset] for annealing cycle 14-CR-1

However, the weldment of 14-CR-2 exhibited better welding performance than 14-CR-1. A plug type nugget failure was obtained and the microstructure of the welded zone was again bainitic martensitic. However, no imperfections were in the weldment (Fig. 5). Further, hardness of the HAZ (390 VPN) was higher than both the welded (353 VPN) and base metal (250 VPN). Thus, there was no HAZ softening and subsequent cracking. This is possibly due to the presence of (Ti-Nb-Mo) CN precipitates that helped control the austenite grain growth in the HAZ, which subsequently resulted in reduced transformed grain size in the HAZ and avoided HAZ softening. Further, the presence of TiC (Fig. 3c) in the HAZ possibly also played a role in controlling the HAZ softening.

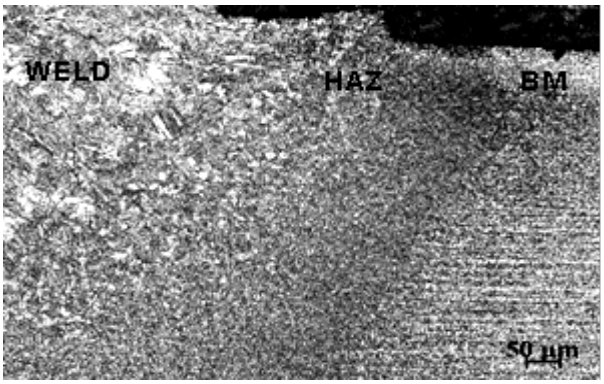

Figure 5. OM micrograph showing defect free weld, heat affected zone (HAZ) and base metal for annealing cycle 14-CR-2

Effect of Bainite--Annealing cycles 9-B-1 and 9-B-2:

a) Microstructure

The base metal microstructure of the cold rolled and continuously annealed sample of cycle 9-B-1 ($10^oC/s$—780^oC (120s)-$2^oC/s$-760^oC-$40^oC/s$—470^oC (60s)-$70^oC/s$) was ferrite with 25% martensite and bainite (Fig. 6a, b). In this case, bainite was quite nominal compared to martensite content. Another annealing cycle, 9-B-2: $10^oC/s$—780^oC (120s)-$2^oC/s$-760^oC-$20^oC/s$—470^oC(60s)-$10^oC/s$ resulted in ferritic-bainitic-martensitic microstructure with bainite and martensite contents of 37%, in which the amount of bainite was relatively more (Fig. 6c). Further, intergranular precipitation of Mo-C was also observed because of slower cooling rate of $20^oC/s$ from quenching temperature to the bainitic temperature (Fig 6d).

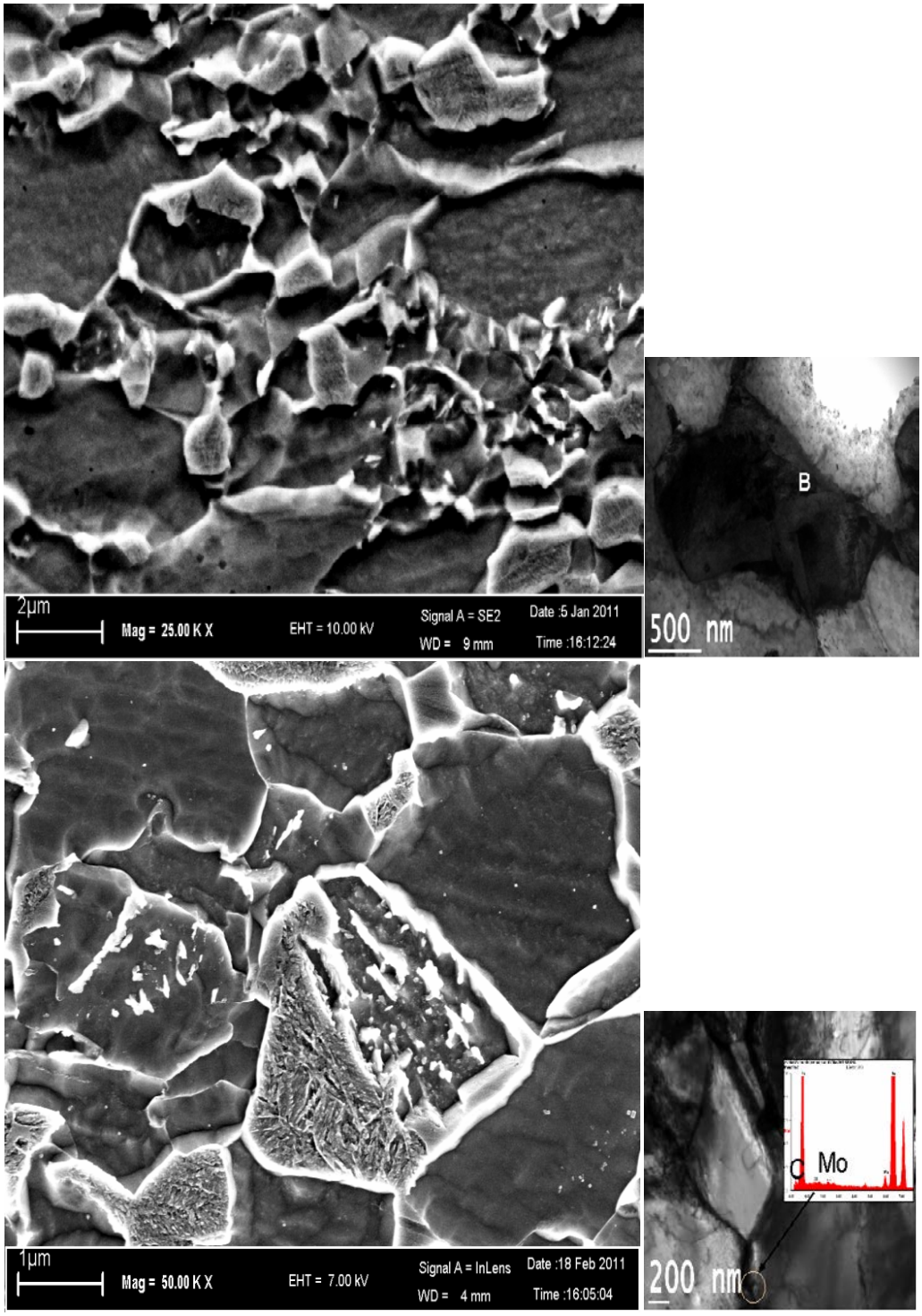

Figure 6. **(a)** FEG-SEM showing ferritic-martensitic-bainiticstructure and **(b)** showing bainite in TEM for annealing cycle 9-2-1, while **(c)** showing ferritic-martensitic-bainitic structure in FEG-SEM and **(d)** and intergranular Mo-C precipitate in TEM for annealing cycle 9-B-2

b) Tensile properties

The YS and TS with 25% M+B in the ferrite matrix of 9-B-1 were obtained as 600 and 702

In this case bainite amount was quite less. The %EL in terms of %UEL and %TEL, was found to be 16 and 23%, respectively, while 'n' value was quite satisfactory with 0.23. The cycle 9-B-2 offered one of the best annealing cycles in the present study with YS and UTS of 449 and 753 MPa with % UEL, %TEL and 'n' as 16%, 22% and 0.18 (Table 4), respectively. This can be attributed to the presence of relatively substantial amount of bainite in association with nano-sized Mo-C precipitates that helped achieve the above properties.

c) Weldability

The 9-B-1 welded sample also resulted in a plug type failure. The welded zone with bainitic-martensitic structure though had no porosities or cracks the HAZ was not devoid of cracks (Fig. 7a). Short cracks in the HAZ were again found to have initiated and propagated at the MnS stringers. Crack generation in the HAZ can be attributed by HAZ softening[8,9]. The hardness of the HAZ was recorded to be 250 VPN while the hardness values of the weld and base metal were 330 and 300 VPN, respectively. On the other hand, 9-B-2 sample was welded successfully with pull-out nugget failure without any weld imperfection and HAZ cracking (Fig. 7b). The successful welding can be attributed to the presence of relatively substantial amount of bainite in the base metal microstructure that helped avoid HAZ softening (HAZ—360 VPN, Weld 355 VPN, base metal—244 VPN) by providing a formable base metal to accommodate the plastic residual stresses during weld cooling. Further, the presence of the carbide forming alloying element like Mo (Mo-C) was possibly able to increase the resistance to HAZ softening[31].

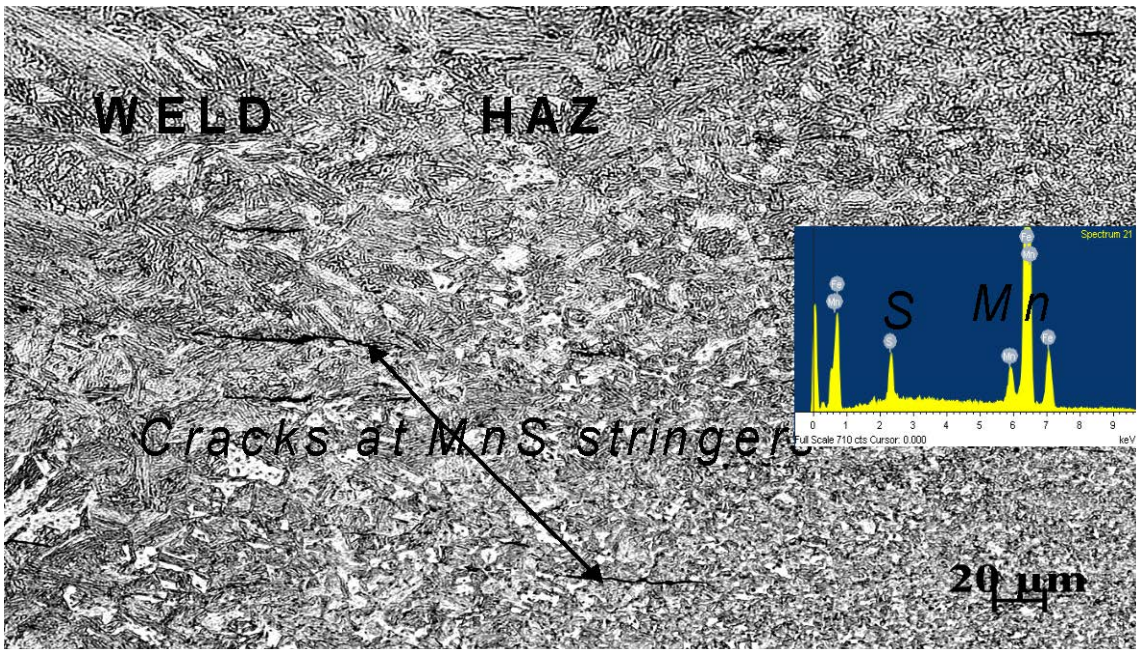

(a)

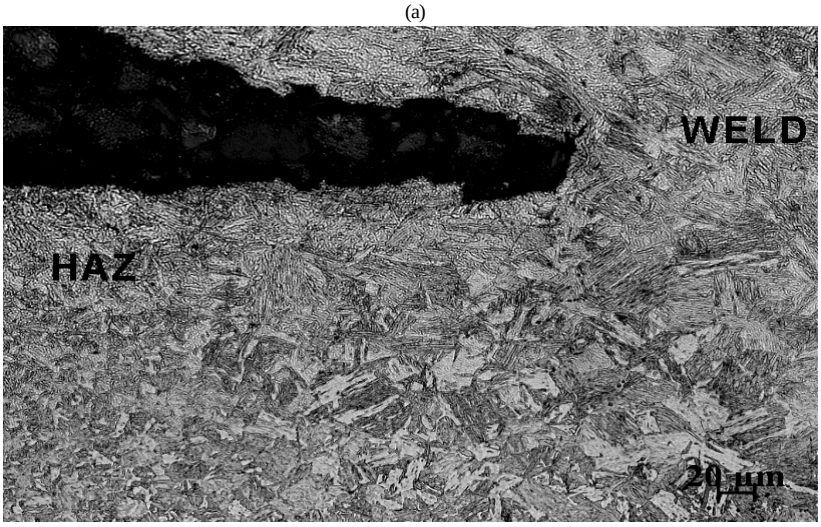

(b)

Figure 7. **(a)** OM micrograph showing HAZ crack in the weldment of 9-B-1 annealing cycle while **(b)** showing defect free weldment for 9-B-2 annealing cycle

From the investigation it is clear that the base metal microstructure played an important role in affecting tensile properties and weldability of the steels. It was inferred that weld HAZ hardness needed to be higher than the weld metal (i. e.$H_{HAZ} > H_{WM}$) while the same requires to be stronger than the base metal also to avoid HAZ softening and thus HAZ cracking.

4. Conclusions

• The steels developed were in the range of ~690-753 MPa ultimate tensile strength and 19-27% total elongation.

• In all the annealing conditions the desirable plug type nugget failure was observed

• Microstructure containing martensite >~ 30% in the base metal and cooling rate of >30^{o}C/s from intercritical annealing temp., (without bainite effect) adversely affected weldability.

• Introduction of optimum amount of bainite in the ferrite and martensite structure resulted in satisfactory weldability behaviour.

• Nano-sized precipitates like TiC, Mo-C and (Ti-Nb-Mo)CN helped obtain desirable tensile and weld properties.

• HAZ softening was found to be the main cause for HAZ cracking. HAZ softening was associated with high martensite (> 30% content) in the base metal.

• In weldments where $H_{HAZ} < H_{WELD}$ and H_{BM} (HAZ softening), liquation cracks and cracks at MnS stringers in HAZ/HAZ-WM were observed.

• Cycle 9-B-2 (10^{o}C/s—780^{o}C (120s)-2^{o}C/s-760^{o}C-20^{o}C /s—470^{o}C (60s)-10^{o}C/s) with ferrite, 37% bainite and martensite along with nano-sized precipitates of Mo-C resulted in the best combination of tensile properties: YS-449 MPa , UTS-753 MPa, %UEL-16%, %TEL-22% and n-0.18, and weldability with plug type nugget failure.

• Stronger HAZ than weld metal in association with formable base metal resulted in favourable combination of stength-ductility-weldability.

ACKNOWLEDGEMENTS

The author is thankful to the management of Tata Steel for permission to publish the work. Special thanks are due to Dr. Vinod Kumar, RDCIS SAIL Ranchi and IIT Madras, for strip annealing tests and TEM examination, respectively.

REFERENCES

[1] V. Cuddy et al, “Manufacturing guidelines when using ultrahigh strength steels in automotive applications, EU report-ECSC R585, 2004.

[2] V. H. Lopez-Cortez and F. A. Reyes-Valdes, Welding Journal, Dec 2008, 36-40.

[3] C. Elgohen, A. De Paepe, A. Lucas and Y Hardy, Materials Sci Forum, Vols 539-543, 2007, p. 4405.

[4] B Girvin, W Peterson and J. Gould, Report on Development of appropriate spot welding practice for Advanced High Strength steels, Project No. 47819GTH, EWI, 1250 Arthur E Adams Drive Columbus, OF 43221, Nov 10, 2004.

[5] J. E. Gould, S. P. Kurana and T. Li, Weld J, May 2006, p.111.

[6] K. Osawa, Y. Suzuki and S. Tanaka, Kawasaki Steel Technical Report, No. 48, March 2003, p.9.

[7] Committee on Automotive applications: “AHSS-application guidelines”, 2006, Washington, DC, Int. Iron and Steel Institute.

[8] J. E. Gould, L. R. Lehman and S. Homes, A. Design of experiments evaluation of factors affecting the resistance spot weldability of high strength steels. Proc Sheet Metal Welding Conf. VII, 1996, AWS Detroit Section.

[9] J. E. Gould and D. Workman, Fracture morphologies of resistance spot welds exhibiting hold time sensitivity behaviour, Proc. Sheet Metal Weld Conf VII, 1998, AWS Detroit Section.

[10] M. V. Li, P. Dong and M. Kimchi, 1997, Modelling and analysis of microstructure development in resistance spot welds of high strength steels, 981BECC-8.

[11] Z. Feng, S. S. Babu, B. W. Riemer, M. L. Santella, J. E. Gould, and M. Kimchi, “Modeling of resistance spot welds: Process and Performance.” 2001, Welding in the World, 45 p.18.

[12] H. Shao, 2000, Blank welding high strength steels, Ph.D. dissertation, Columbus, Ohio, The Ohio State Univ.

[13] S. L. Ream, 2003, Remote laser weld performance in advanced high strength steels. Proc. ALAW 2003, Univ. of Michigan.

[14] W. L. Chuko and J. E. Gould, Weld J., 2002, p.1s.

[15] M. Milititsky, E. Pakalnins, C. Jiang, A. K. Thompson, On Characteristics of DP600 resistance spot welds, SAE Report, Paper No. 01-0520, Detroit, 2003.

[16] C. Ma, S. D. Bhole, D. L. Chen, A. Lee, E. Biro, G. Boudreau, Sci. Technol, Weld Joining, 11, 2005, p.296.

[17] M. I. Khan, M. M. L. Kuntz, P. Su, A. Gerlich, T. North and Y. Zhou, Sci. Technol. Weld Joining, 2007, 12, p.175.

[18] G. Wang & M. E. Barkety, Weld. J., 85, 2006, p.84s.

[19] M. Maryas and X. Q. Gayden, Weld. J., 84, 2005, p.172s.

[20] A. Joaquin, A. Elliot, C. Jiang, Weld. J., 2007, Vol. 86, No. 2, p. 24s.

[21] M. Marya, and X. Q. Gayden, Weld J, 2005, 84, No 11, p.172.

[22] V. H. Baltazar Hernandez, M. L. Kuntz, M. I. Khan and Y. Zhou, Sci. and Technol. of Welding & Joining, 13, No. 8, 2008, p.769.

[23] M. I. Khan, M. L. Kuntz and Y. Zhou, Sci. Technol. Weld Joining, 2008, 13, p.49.

[24] S. Hashimoto, S. Kanbe and M. Sudo, Trans. ISIJ, 1981, 21,

p.B-497.

[25] N. Yamauchi, T. Taka, K. Kunishige and N. Nagao, Trans ISIJ, 1982, 22, B-107.

[26] E. Biro and A. Lee, Sheet Metal Welding Conf XII, AWS, Livonia, MI, 2006.

[27] M. Xia, E. Biro, Z. Tian and Y. N. Zhou, ISIJ, 2008, 48, p.809.

[28] S. Dancette, V. Massardier-Jourdan, D. Fabregue, J. Merlin, T. Dupuy and M. Bouzekri, Isij Int, 51, No 1, 2011, p.99.

[29] B. Hemsworth, T. Boniszewski and N. F. Eaton, Classification and definition of high temperature welding cracks in alloys. Metallurgy, Feb 1969, p.5.

[30] K. Banerjee, N.L. Richards and M.C. Chaturvedi, Metall. and Mater. Trans. A, Vol 36A, July, 2005, p.1881.

[31] E. Biro, J.R. McDermid, J.D. Embury, and Y.Zhou, Metall. and Mater. Trans. A, Vol. 41A, Sept, 2010, p.2348.